CHEMISTRY OF MATERIALS

ARTICLE

pubs.acs.org/cm

A Novel Polyimide Dispersing Matrix for Highly Electrically Conductive Solution-Cast Carbon Nanotube-Based Composite

Wei Yuan, Jianfei Che, and Mary B. Chan-Park*

School of Chemical and Biomedical Engineering, Nanyang Technological University, 62 Nanyang Drive, Singapore 637459, Singapore

Supporting Information

ABSTRACT: Multiwalled carbon nanotubes (MWNTs) have high intrinsic conductivities and are thought to be ideal fillers for electrically conductive composites. However, so far, simple solution casting or blending of nanotubes has not been highly successful in producing highly conductive composites, because of the poor dispersion and low loading of the nanotubes. We show that, by using a novel poly(amic acid) (PAA) containing a rigid backbone with hydroxyl pendant groups, as both the nanotube dispersant and the matrix precursor, we can increase the nanotube content in the solution-cast polyimide (PI)-based composite to as high as 30 wt % and achieve ultrahigh composite electrical conductivity as well as high mechanical properties. The electrical conductivity of the MWNT/PI composites reaches a value of 38.8 S cm^{-1} at a nanotube loading of 30 wt % and the MWNT concentration for achieving the percolation threshold of conductivity of the composites is 0.48 wt %. These are, respectively, the highest and among the lowest reported values for any conventional solution-processed nanotube composites. The 30 wt % MWNTs composite has a higher Young's modulus (9.43 ± 0.14 GPa) and tensile strength (179.2 ± 9.7 MPa) than other nanotube-reinforced polyimide composites. The high conductivity, as well as tensile properties, of the composite films is attributed to the good nanotube dispersion and strong nanotube−polymer interfacial adhesion achieved through use of a single polymer to perform the dual functions of nanotube dispersant and matrix precursor. The excellent properties, combined with the facile conventional solution-casting technique, make this MWNT/PI composite film a promising material for many potential applications. We have also demonstrated that uniform MWNT(30 wt %)/PI composite coatings can be deposited onto glass and aluminum substrates.

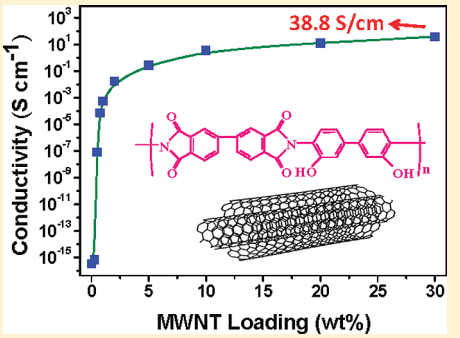

KEYWORDS: multiwalled carbon nanotubes, noncovalent functionalization, polyimide, electrical conductivity, mechanical properties

INTRODUCTION

Because of their excellent electrical conductivity (10^3−10^6 S cm^{-1}), ultrahigh strength, large aspect ratio, and low density, carbon nanotubes (CNTs) are considered to be an ideal additive for making high-performance conductive polymer composites.[1,2] On the other hand, polymer composites used in engines, ducts, machinery, aircraft parts, etc. often must be electrically conductive, as well as lightweight and structurally strong and stiff, in order to confer antistatic and electromagnetic shielding properties. Many studies on increasing the electrical conductivity of CNT/polymer composites have been published.[3−7] Very high electrical conductivities (17−200 S cm^{-1})[5−7] have been obtained in some composites with a CNT content above 75 wt %; however, these employed special nanotubes[7] and/or nonconventional composite processing techniques, such as vacuum filtration[5,6] or coagulation spinning,[7] which allow high nanotube content and alignment. However, typical composite processing techniques such as casting, resin transfer molding, etc. often must be employed to make composites, because of cost, shaping, functional, or other requirements. With these techniques, the electrical conductivity achieved with CNT loading has generally been modest. Few studies[3,8] have reported composites with electrical conductivities of >1 S cm^{-1}. Ramasubramaniam et al. reported a conductivity of 4.81 S cm^{-1} with polycarbonate,[3] and Grossiord et al. reported a conductivity of 10 S cm^{-1} with vertically aligned nanotubes.[8] Furthermore, high-performance conductive composites made from solution casting have not been reported.

Polyimides (PIs) are an important class of structural polymers that are widely used in the microelectronics and aerospace industries, because of their outstanding thermal stability and mechanical properties. The electrical conductivities achieved in polyimide/CNT composites have typically been low. Jiang et al.[9] reported a conductivity of ∼10^{-1} S cm^{-1} for a nanotube/polyimide composite with 5 wt % nanotubes. Further improvement in electrical conductivity in solution-processed polyimide/CNT composites, like most other similarly processed composites, has been hampered by low CNT content (≤10 wt %)[9−14] and poor dispersion of the CNTs. It has generally been thought that highly electrically conductive composites can be achieved if the CNT content is high and the nanotubes are well-dispersed within the polymer matrix, so that they are percolative. To debundle and disperse the CNTs as individual tubes, covalent

Received: March 30, 2011
Revised: August 10, 2011
Published: August 29, 2011

and noncovalent approaches can be used;[1,15,16] however, noncovalent functionalization is preferable, because it preserves the graphene structure of the nanotubes and, consequently, their intrinsic electrical and mechanical properties. We and other researchers have explored polymers as noncovalent dispersants of CNTs.[15,17,18] However, most work on CNT composites has utilized a polymeric dispersant that is distinct from the matrix.[3,19−21] This approach tends to limit the CNT loading in the matrix to low content (e.g., 10 wt %), since, at high CNT loading and, therefore, polymeric dispersant loading, incompatibility between the dispersant and matrix promotes CNTs aggregation, particularly during removal of the solvent used to dissolve the matrix and the dispersed CNTs. We hypothesize that the use of a single polymer, which can serve as both nanotube dispersant and matrix (or matrix precursor), is a more effective way to achieve composites with high CNT content. The polymer must be able to disperse the CNTs and also provide the desired properties of the matrix. This method should yield the best possible compatibility between the CNTs and the polymer matrix, and therefore would prevent CNT aggregation during the processing of high-nanotube-content composites.

In this paper, we demonstrate a high performance multiwalled carbon nanotube (MWNT)-reinforced polyimide composite film prepared by solution casting with excellent conductivity and high mechanical properties. A novel poly(amic acid) (PAA) (see Figure 1a) was designed and synthesized to act as both the MWNT dispersant and matrix precursor. Solution-cast and thermally imidized MWNT/PI composite film with 30 wt % nanotubes has an electrical conductivity of 38.8 S cm^{-1} (compared to an electrical conductivity of 3.5 × 10^{-16} S cm^{-1} for the neat polyimide). This composite has a Young's modulus of 9.43 ± 0.14 GPa and a tensile strength of 179.2 ± 9.7 MPa, both of which are higher than other reported values for polyimide. Uniform MWNT(30 wt %)/PI composite coatings were also successfully deposited on glass and aluminum substrates.

EXPERIMENTAL SECTION

Materials. MWNTs with a diameter of 10−15 nm and a length of 10−20 μm were supplied by Iljin Nano Tech, Korea. They were purified via thermal oxidation at 350 °C for 2 h in air, followed by refluxing in 6 M HCl solution overnight. 3,3′-Dihydroxy-4, 4′-diaminobiphenyl (HAB, 97%) was purchased from Tokyo Chemical Industry and purified by recrystallization from *N*,*N*′-dimethylformamide (DMF)/ethanol mixture. 3,3′,4,4′-biphenyltetracarboxylic dianhydride (BPDA), poly(vinyl pyrrolidone) (PVP, M_w = 29 000), *N*,*N*′-dimethylacetamide (DMAc), and all other chemicals were obtained from Sigma−Aldrich. BPDA was purified via sublimation under reduced pressure. DMAc was distilled over calcium hydride. All other chemicals were used without purification.

Synthesis of Poly(amic acid) (PAA). Typically, a solution of HAB (2.16 g, 10 mmol) in freshly distilled DMAc (51 mL) was added into a 100-mL three-necked flask under flowing argon. After the HAB was completely dissolved, BPDA (2.94 g, 10 mmol) was added at 0 °C and the mixture was mechanically stirred at room temperature for 24 h. The resulting viscous PAA solution was kept in a freezer until use. The molecular weight of PAA determined by GPC was M_w = 1.97 × 10^5 g/mol with a polydispersity index of 1.96.

Fabrication of MWNT/PI Composite Films. A measured quantity of MWNTs was added into DMAc (the concentration

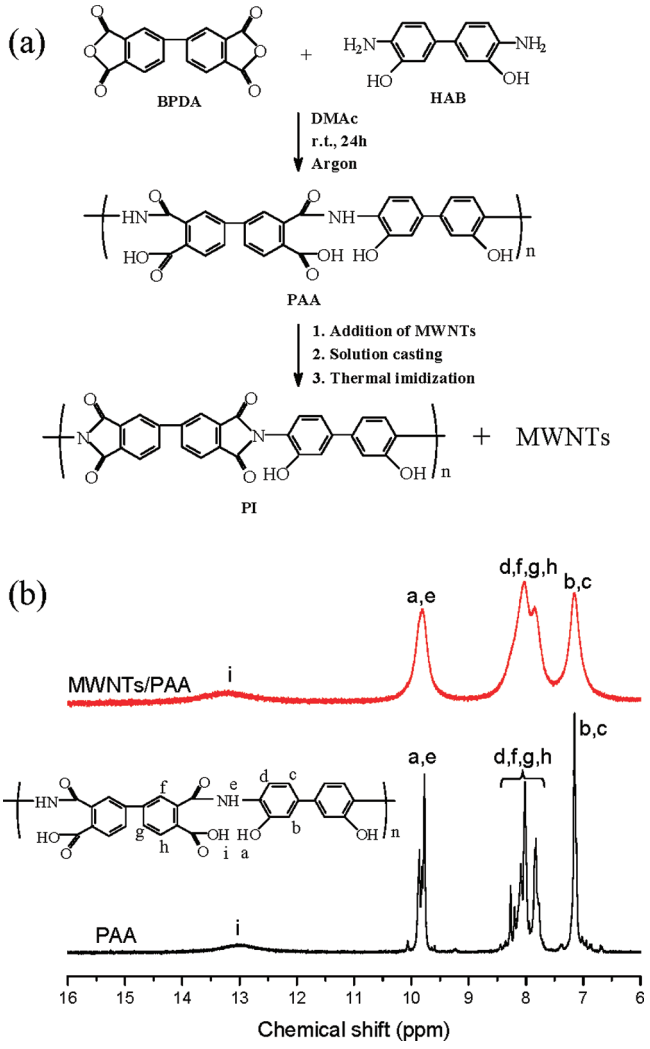

Figure 1. (a) Synthesis of poly(amic acid) (PAA) and the strategy for fabricating MWNT/polyimide composites. (b) ^{1}H NMR spectra of PAA and MWNTs/PAA (mass ratio of 1:2) in DMSO-d_6.

of MWNTs in DMAc was fixed at 1 mg/mL), and the mixture was sonicated with a high-power tip sonicator (500 W, 35%, Vibra-Cell Sonics) for 5 min. Different quantities of PAA solution then were mixed with the MWNT/DMAc suspension and sonicated with the tip sonicator for another 5 min, followed by further sonication in a low-power sonication bath (S30H, Elma) for 30 min at 0 °C. MWNT/PAA dispersions with <10 wt % MWNTs were directly cast into films. Dispersions with 10−30 wt % MWNTs were prepared with a large amount of DMAc, some of which was slowly evaporated in a glass dish before film casting. No obvious nanotube aggregates were observed by eye and via optical microscopy (200× magnification) (see Figure S1 in the Supporting Information) during this process. The MWNT/PAA dispersions were cast onto glass slides, which were heated on a hot plate at 50 °C. After the removal of most of the DMAc, the glass slides were transferred to a vacuum oven and dried at 80 °C under vacuum for 3 h to remove residual solvent. Finally, the as-prepared MWNT/PAA films were imidized under argon at 100 °C for 2 h, 200 °C for 1 h, 300 °C for 1 h, and 350 °C for 20 min. The thickness of the resulting films was measured to be 15 ± 1 μm. The MWNT volume fraction was computed from its mass fraction,

dx.doi.org/10.1021/cm200909x |*Chem. Mater.* 2011, 23, 4149–4157

based on the MWNT true density (2.15 g cm^{-3}) and the polyimide density (1.4 g cm^{-3}).

Fabrication of MWNT/PI Composite Coatings. Ultrathin MWNT/PAA coatings on the glass and aluminum substrates were fabricated from MWNT(30 wt %)/PAA dispersion (nanotube concentration of 0.1 mg/mL) using an air brush (Badger, model 100LG). During the spray process, the substrates were kept on a hot plate at ~170 °C, in order to accelerate the evaporation of DMAc. The nozzle was kept at a distance of 20−30 cm from the substrates, and the dispersion was sprayed, one spray at a time, onto the substrates. A thick MWNT(30 wt %)/PAA coating on the aluminum was prepared by solution casting. MWNT/PI coatings were obtained after thermal imidization.

Characterization. ^{1}H NMR spectra of PAA and MWNTs/PAA were obtained with a Bruker Avance 300 NMR spectrometer, using deuterated dimethylsulfoxide (DMSO-d_6) as the solvent and tetramethylsilane as the internal standard. The weight-average molecular weight (M_w) and polydispersity (PDI) of poly(amic acid) was measured via gel permeation chromatography (GPC) that was performed with a Shimadzu LC-20A Series GPC system equipped with a pump, a BC-PL gel mixed column, and a RID-10A refractive index detector, using DMF with 0.02 M LiBr as eluent and polystyrene standards as reference. Raman characterization was carried out on a Renishaw Ramanscope with HeNe laser at an excitation wavelength of 633 nm. The absorption spectra of PAA- or PVP-dispersed MWNT dispersions, and the transmittance of an ultrathin composite coating on glass, were measured by a Varian Cary 5000 UV−vis−NIR spectrophotometer. Atomic force microscopy (AFM) was conducted, using a MFP 3D microscope in ac mode. A pristine MWNT suspension or MWNT/PAA (mass ratio = 1:2) dispersion in DMAc was prepared via sonication and then deposited onto a clean silicon wafer by spin coating. High-resolution transmission electron microscopy (TEM) images were obtained using a JEOL Model 3010F analytical electron microscope operating at an accelerating voltage of 300 kV. TEM samples were prepared by placing several drops of pristine MWNT suspension or MWNT/PAA (mass ratio = 1:2) dispersion in DMAc on a carbon-coated copper grid and drying at room temperature. Field-emission scanning electron microscopy (FE-SEM) analysis was performed with a JEOL Model JSM-6700F microscope operating at 5 kV. Composite films were fractured in liquid nitrogen, and the cryofractured surfaces were sputter-coated with gold. Tensile tests of cast films were conducted with an Instron Model 5543 mechanical tester at ambient temperature, with a gauge length of 20 mm and a crosshead speed of 2 mm/min. At least five specimens from each batch were tested. Electrical conductivity was measured by a two-probe method using a Keithley Model 610C electrometer at room temperature. Silver paste was applied onto two ends of measured samples to ensure good electrical contact between the electrodes and the sample.

RESULTS AND DISCUSSION

Design and Synthesis of PAA. The PAA (Figure 1a) was synthesized from HAB and BPDA, using stoichiometric amounts of these compounds to achieve the highest molecular weight possible. High molecular weight enables more contact points between the polymer molecules and CNTs, to increase the CNT dispersion efficacy.[22,23] The biphenyl diamine and dianhydride polymerize to a rigid and unbent PAA backbone, which facilitates the stacking of the dispersant molecules onto the conjugated MWNT surface via $\pi-\pi$ interaction,[24] to promote PAA adsorption and produce a relatively strong bond between the dispersant and the MWNTs. The pendent −OH and −COOH groups provide the functionalized MWNTs with good solubility in organic solvents and a polymer matrix precursor.

The ^{1}H NMR spectrum of PAA in DMSO-d_6 (see Figure 1b) confirms its successful synthesis with the characteristic aromatic proton peaks at δ 7.1−7.2 ppm (peaks b and c) and 7.8−8.3 ppm (peaks d, f, g, and h), the phenolic −OH and −NH protons peaks at δ 9.7−9.9 ppm (peaks a and e) and the −COOH proton peak at δ 13.0 ppm (peak i). Interaction with the nanotube π cloud is known to cause ^{1}H NMR signal broadening.[17,20,25] Such broadening is evident in the MWNTs/PAA (mass ratio = 1:2) spectrum (see Figure 1b). The interaction between MWNTs and PAA is so strong that PAA cannot be completely washed away by DMAc, which is a good solvent for PAA (which is evident from Fourier transform infrared (FT-IR) spectra, shown in Figure S2 in the Supporting Information). The percentage of PAA that cannot be washed away was calculated to be ~23%, from thermogravimetric analysis (TGA) (see Figure S3 in the Supporting Information).

PAA converts to PI after thermal imidization. The differential scanning calorimetry (DSC) curve of PAA film (seeFigure S4 in the Supporting Information) shows that the imidization process mainly occurs in the temperature range of 150−180 °C, which is covered by our heating range (from 100 °C to 350 °C). We heated to a temperature of 350 °C, to maximize the degree of imidization. It is necessary to note that further heating to 400 °C should be avoided, because the −OH groups in PI can result in thermal conversion of PI to polybenzoxazole upon heating over this temperature in an inert atmosphere.[26,27] There is no observation of cross-linking reaction between pendant −OH groups,[27] which is possibly due to the strong steric hindrance.

Dispersion of MWNTs/PAA in DMAc. When pristine MWNTs are dispersed in DMAc and allowed to stand for one week, the MWNTs mostly settle at the bottom of the vial (see Figure 2, vial a). The addition of PAA (Figure 2, vial b) results in homogeneous dispersions of MWNTs/PAA without visible aggregates anywhere in the vial, even after several months of standing (Figure 2, vials c and d). The maximum MWNT concentration that can be dispersed with PAA was determined to be ~2.8 mg/mL, which is comparable to the highest reported values with other dispersants (2.5−3 mg/mL).[20,23]

The efficacy of PAA at dispersing MWNTs in DMAc was quantitatively evaluated and compared with that of poly(vinyl pyrrolidone) (PVP), which is a commercially avaliable dispersant for nanotubes,[28] through absorbance measurements and the Beer−Lambert law. Nanotube concentration can be determined by the Beer−Lambert law,

$$A = \varepsilon l c$$

where A is the absorbance at a particular wavelength, ε the extinction coefficient, l the light path length (l = 1 cm for our cell), and c the nanotube concentration.[22] To determine the value of ε, the absorbance spectra of very dilute and well-dispersed MWNT/PAA (mass ratio 1:2) dispersions at different concentrations were measured (see Figure 3a) and the absorbance at 500 nm was plotted against nanotube concentrations (see inset in Figure 3a). The linear-least-squares fit to the data gave a slope of 0.04704, so the extinction coefficient was calculated to be 0.04704 L mg^{-1} cm^{-1}, which is in agreement with those found at

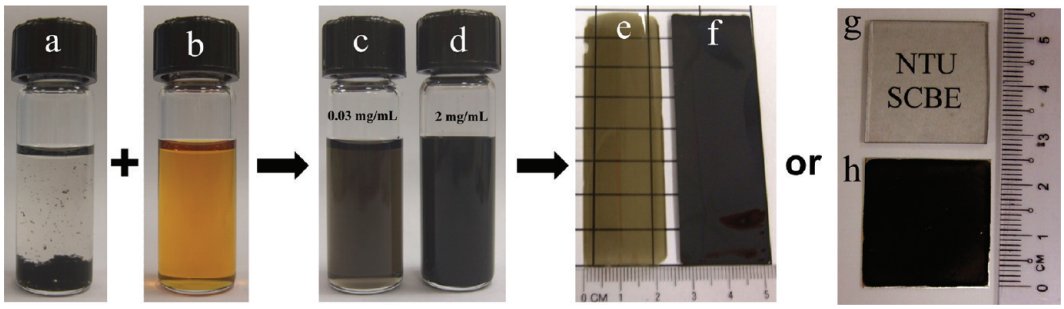

Figure 2. Photographs of (a) pristine MWNTs, (b) PAA solution, (c and d) PAA-functionalized MWNT dispersions, (e and f) MWNT/PI composite films with nanotube loadings of 0.25 wt % (panel e) and 30 wt % (panel f), and (g and h) MWNT/PI coatings on glass substrates (panel g) and aluminum substrates (panel h).

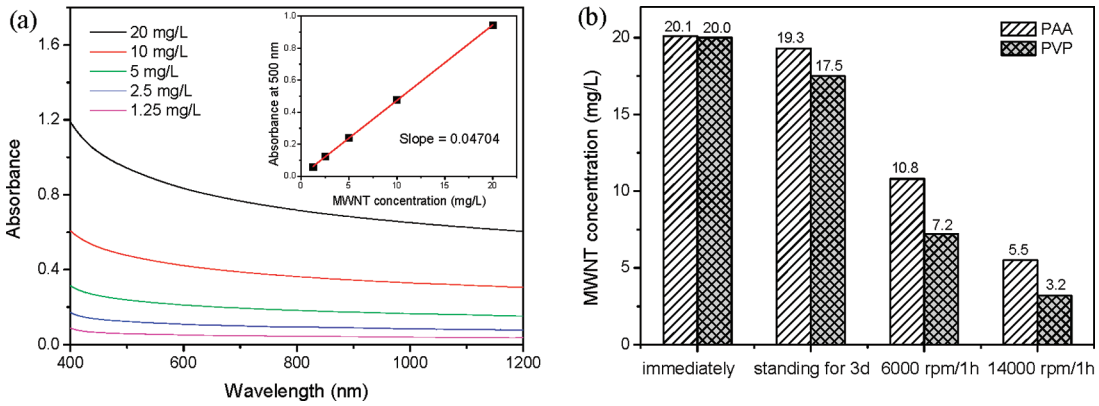

Figure 3. (a) Absorption spectra of MWNTs/PAA (mass ratio = 1:2) in DMAc at different nanotube concentrations. Inset shows the absorbance of these dispersions at 500 nm. The straight line is a linear-least-squares fit to the data. (b) MWNT concentrations of MWNTs/PAA (mass ratio = 1:2) and MWNTs/PVP (mass ratio = 1:2) under different conditions: immediately after sonication, after standing for 3 days, after centrifugation at 6000 rpm for 1 h, and after centrifugation at 14 000 rpm for 1 h.

500 nm for MWNTs in chloroform (0.04220 L mg^{-1} cm^{-1})[22] and *o*-dichlorobenzene (0.04600 L mg^{-1} cm^{-1}).[29] The nanotube concentrations of MWNTs/PAA (mass ratio = 1:2) and MWNTs/PVP (mass ratio = 1:2) under different conditions, determined using absorbance at 500 nm and the Beer−Lambert law, are shown in Figure 3b. Immediately after sonication, both MWNTs/PAA and MWNTs/PVP have nanotube concentrations of ~20.0 mg/L. After standing for 3 days, centrifugation at 6000 rpm for 1 h and centrifugation at 14 000 rpm for 1 h, the nanotube concentration of MWNTs/PAA decreases to 19.3, 10.8, and 5.5 mg/L, respectively, which is higher than that of MWNTs/PVP (17.5, 7.2, and 3.2 mg/L, respectively), suggesting higher efficacy of our PAA than PVP at dispersing MWNTs in DMAc.

TEM images further show the high efficacy of PAA at dispersing MWNTs (Figure 4). Pristine MWNTs, which are used as controls, form large aggregates (see Figure 4a), while the majority of the PAA-dispersed MWNTs are observed as individual tubes (see Figure 4c). At the higher magnification, the pristine MWNT surface is quite clean (see Figure 4b), while there is an amorphous coating layer with a thickness of 1−2 nm in MWNTs/PAA (see Figure 4d). We interpret this feature of Figure 4d to be a layer of PAA that has self-assembled onto the nanotube surface, which contributes to long-term stability and individually dispersed MWNTs.

The capability of PAA at dispersing MWNTs into individual tubes was also manifested by the AFM image. As shown in Figure 5, most of the PAA-dispersed MWNTs have lengths of >2 μm, indicating that noncovalent functionalization of MWNTs with PAA does not significantly reduce the nanotube length.

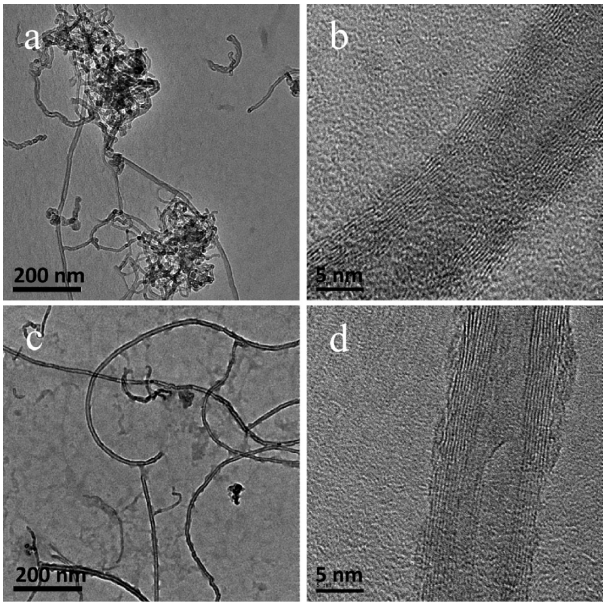

Figure 4. TEM images of (a and b) pristine MWNTs and (c and d) PAA-dispersed MWNTs.

dx.doi.org/10.1021/cm200909x |*Chem. Mater.* 2011, 23, 4149–4157

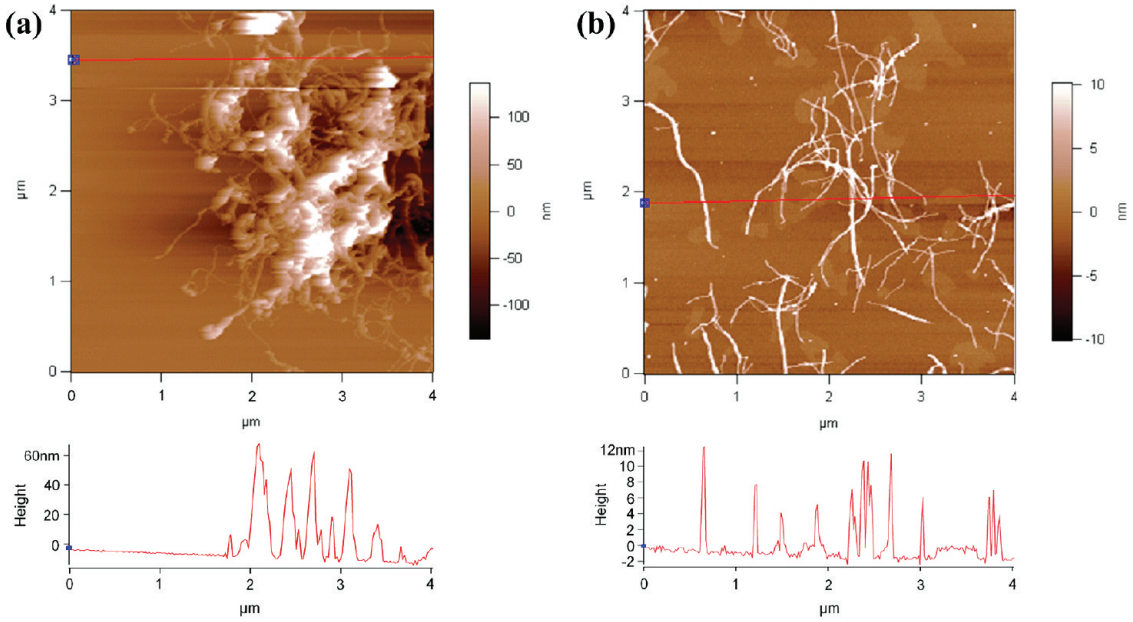

Figure 5. AFM images of (a) pristine and (b) PAA-dispersed MWNTs deposited on silicon wafers by spin coating.

The measured height of the MWNTs is in the range of 8−15 nm, which is close to the diameter of pristine MWNTs (10−15 nm), suggesting that the MWNTs are dispersed as individual tubes. We attribute the high efficacy of PAA at dispersing MWNTs to its unique structure. The rigid unbent highly aromatic backbone of PAA has a strong affinity via $\pi-\pi$ interaction to the highly conjugated graphene-like surface of nanotubes, while the pendent −COOH and −OH groups provide MWNTs with solubility and keep them from reaggregation.

MWNT Dispersion and MWNT-PI Interfacial Bonding in Composite Films. Figures 2e and 2f show representative photographs of composite films containing 0.25 wt % and 30 wt % MWNTs. The composite with 0.25 wt % MWNTs possesses good transparency and uniformity, while the composite with 30 wt % MWNTs is completely opaque. Even under 200× magnification in optical microscopy, no visible aggregates were observed in the MWNT/PI composite films, indicating homogeneous MWNT dispersion (see Figure S5 in the Supporting Information).

To further examine the nanotube dispersion in composite film, MWNT(1 wt %)/PAA film without thermal imidization was redispersed in DMAc with only mild shaking. This dispersion was then filtered through a 0.2-μm Al_2O_3 membrane and washed with a large quantity of DMAc to remove free polymer. FE-SEM images of the MWNTs on the Al_2O_3 membrane (Figure 6) show that the MWNTs are well-dispersed without significantly reduced length. The diameter of MWNTs, which were coated with a layer of gold before FE-SEM observation, is ∼14−20 nm. This value is only 4−5 nm larger than that of pristine MWNTs (10−15 nm), indicating that MWNTs in Figure 6 are dispersed individually. We confirmed that MWNTs cannot be dispersed by PAA with only mild shaking (data not shown), so Figure 6 exhibits the nanotube dispersion state in composite film. The nanotube morphology in Figure 6 suggests that MWNTs can generate a conductive network for electron transport, leading to high electrical conductivity for the final MWNT/PI composite film, which will be discussed below.

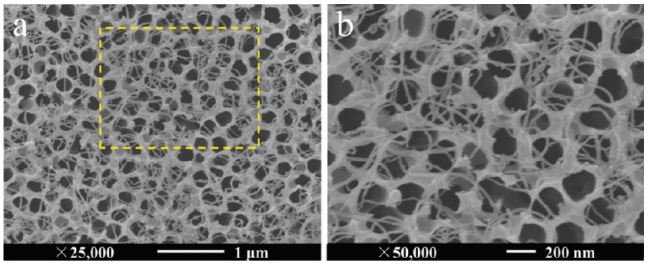

Figure 6. FE-SEM images of MWNTs: (a) MWNT(1 wt %)/PAA composite film on 0.2-μm Al_2O_3 filter membranes after removal of free polymer, and (b) enlarged image of a selected region in panel a.

To investigate the dispersion and morphology of nanotubes in fully imidized MWNT/PI composites, composite films were dipped into liquid nitrogen and then broken. FE-SEM images of cryofractured surfaces of composites with nanotube contents of 1, 10, and 30 wt % are shown in Figure 7. For all three loadings, MWNTs are dispersed homogeneously throughout the surfaces without any obvious aggregates (Figure 7a−f). With 1 wt % MWNTs (Figures 7a and 7b), MWNTs are broken on the surface (indicated by arrows), suggesting strong polymer-nanotube interfacial adhesion. The diameter of the MWNTs in Figure 7b (∼40−60 nm) is much larger than that in MWNT(1 wt %)/PAA composite after removal of polymer (∼14−20 nm; see Figure 6b), suggesting a thick cladding of polymer on the surface of the nanotube.[30,31] The FE-SEM images of MWNT(10 wt %)/PI materials (Figures 7c and 7d) reveal more MWNTs on the surface, compared to the MWNT(1 wt %)/PI sample. Some MWNTs are partially pulled out from the surface, but most MWNTs are broken on the surface and well-wetted by the PI matrix, which is again reflected in the large diameter of the polymer-clad nanotubes (see Figure 7d). As the MWNT content increases to 30 wt % (Figures 7e and 7f), there are more MWNTs "competing" for the matrix, leading to less polymer cladding on the MWNT surface, as reflected in the reduced diameters of the

dx.doi.org/10.1021/cm200909x |*Chem. Mater.* 2011, 23, 4149–4157

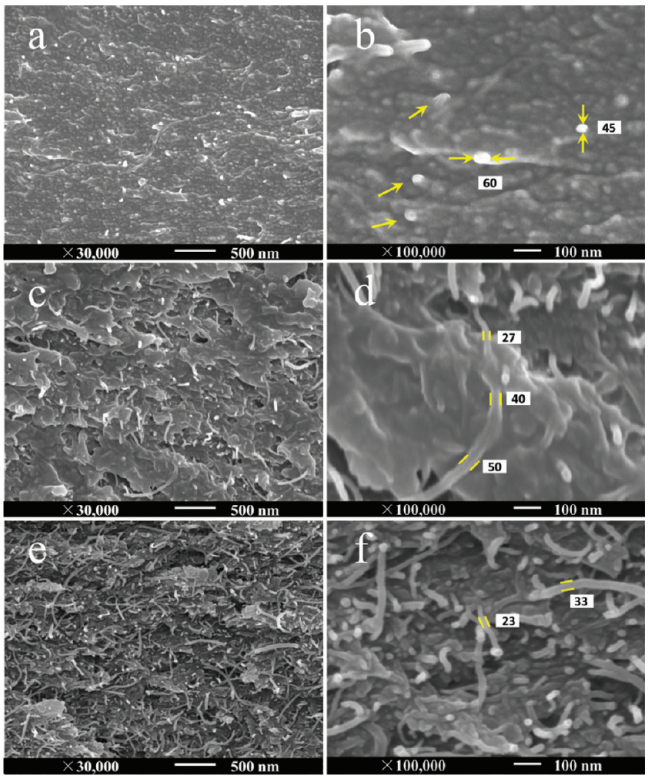

Figure 7. FE-SEM images of cryofractured surfaces of MWNT/PI composite films with MWNT loadings of (a and b) 1 wt %, (c and d) 10 wt %, and (e and f) 30 wt %. Images to the right (panels b, d, and f) show enlarged views of selected areas in the images to the left (panels a, c, and e).

polymer-clad MWNTs (~18−33 nm) and, consequently, more pulled-out MWNTs.

It has been shown that the wrapping of polymer around nanotubes can result in a shift toward higher frequencies of the peak of the tangential vibrational mode (G-band),[20,32] because of charge transfer from the CNTs to the polymer dispersant.[33] Figure 8 shows the Raman spectra of pristine MWNTs and MWNT/PI composites with nanotube contents of 30 wt %, 20 wt %, 10 wt %, and 5 wt %. The disorder mode (D-band) and the tangential mode (G-band) of MWNTs are seen at ~1335 cm^{-1} and ~1600 cm^{-1}, respectively. The G-band peak of pristine MWNTs is located at 1596 cm^{-1} (spectrum a), while that of MWNT/PI composites with a MWNT content of 10−30 wt % are located at ~1611 cm^{-1} (spectra b−d). The observed 15 cm^{-1} Raman upshift in MWNT/PI composites confirms the presence of strong $\pi-\pi$ interaction between PI and MWNTs. Moreover, the Raman peaks become less distinct as the MWNT content in composites decreases from 30 wt % to 10 wt %. In MWNT/PI composites with nanotube loadings of 0.25−5 wt %, the Raman spectra features are overwhelmed by the strong broad luminescence background and the characteristic peaks of MWNTs are undetectable (here, we show only the spectrum of the 5 wt % MWNT sample, spectrum e), which has also been observed in other functionalized CNTs.[34,35] It has been suggested that a better nanotube dispersion enhances the luminescence, leading to more-significant interference in Raman measurements.[36] Thus, the strong luminescence observed in our composites with 0.25−5 wt % MWNTs suggests good nanotube dispersion without significant aggregation.

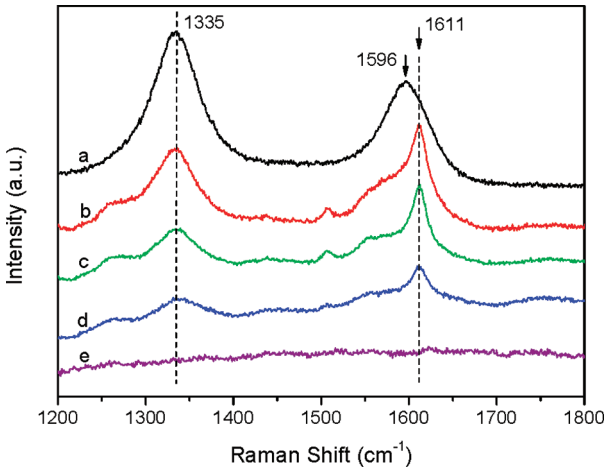

Figure 8. Raman spectra of (a) pristine MWNTs, and MWNT/PI composites with MWNT loadings of (b) 30 wt %, (c) 20 wt %, (d) 10 wt %, and (e) 5 wt %.

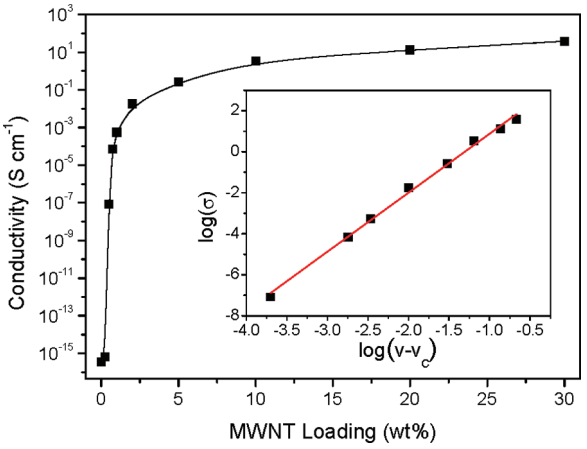

Figure 9. Log DC conductivity, measured at room temperature, as a function of MWNT mass fraction for MWNT/PI composites. The inset shows the best fit to the conductivity data using the equation described in the text for the determination of percolation threshold.

Electrical Conductivity. Figure 9 and Table 1 show the DC conductivity of MWNT/PI composites, measured at room temperature, as a function of MWNT loading. The conductivity of neat PI is 3.5 × 10^{-16} S cm^{-1} and no obvious increase is observed with the addition of 0.25 wt % MWNTs. As the MWNT loading increases from 0.25 wt % to 0.5 wt %, the conductivity exhibits a sharp increase of ~8 orders of magnitude, from 6.8 × 10^{-16} S cm^{-1} to 8.3 × 10^{-8} S cm^{-1}, indicating the formation of a percolating network. Percolation theory predicts that the composite conductivity versus nanotube volume fraction obeys the power law:[37]

$$\sigma \propto (v - v_c)^t \qquad \text{for } v > v_c$$

where σ is the composite conductivity, v the nanotube volume fraction, v_c the percolation threshold, and t the critical exponent. The best fit of our experimental electrical conductivity data to the above equation gives a value of v_c = 0.31 vol % (i.e., 0.48 wt %) and t = 2.8 with a correlation coefficient of 0.9954, as shown in the plot of $\log(\sigma)$ versus $\log(v-v_c)$ in the inset in Figure 9.

dx.doi.org/10.1021/cm200909x |*Chem. Mater.* 2011, 23, 4149–4157

Table 1. Mechanical and Electrical Properties of Neat PI and MWNT/PI Composite Films

CNT Loading					
[wt %]	[vol %]	modulus [GPa]	strength [MPa]	elongation [%]	conductivity [S cm^{-1}]
0	0	6.37 ± 0.13	151.2 ± 5.1	4.5 ± 0.2	3.5×10^{-16}
0.25	0.16	7.30 ± 0.09	175.0 ± 6.3	6.2 ± 0.3	6.8×10^{-16}
0.5	0.33	7.68 ± 0.12	188.1 ± 3.4	5.9 ± 0.4	8.3×10^{-8}
0.75	0.49	8.15 ± 0.09	193.6 ± 6.5	5.6 ± 0.2	7.2×10^{-5}
1	0.65	8.47 ± 0.17	206.7 ± 6.8	5.4 ± 0.3	5.6×10^{-4}
2	1.31	8.88 ± 0.11	215.4 ± 5.2	5.0 ± 0.3	1.8×10^{-2}
5	3.31	9.21 ± 0.07	221.3 ± 6.3	4.4 ± 0.3	0.27
10	6.75	9.55 ± 0.12	228.4 ± 5.2	4.1 ± 0.2	3.5
20	14.00	9.97 ± 0.13	206.6 ± 4.0	3.2 ± 0.1	13.3
30	21.82	9.43 ± 0.14	179.2 ± 9.7	2.5 ± 0.3	38.8

Our percolation threshold (0.48 wt %) is much lower than most reported values for CNT/polyimide composites (>1 wt %).[10−12,14,38,39] In most reported methods of preparation of CNT/PI composites, CNTs are modified by acid treatment, which has been shown to reduce CNT intrinsic electrical conductivity, because of the introduced structural defects. Furthermore, decreased nanotube length and aspect ratio of acid-treated CNTs lead to a higher CNT fraction needed to form a continuous charge carrier channel in composites. As a result, relatively high percolation thresholds were observed in these studies. In our method, the designed PAA molecular chains are adsorbed onto the MWNT surface to disperse nanotube bundles into individuals without any substantial damage to the MWNT length and structure. The original aspect ratio and intrinsic electrical properties of the MWNTs are better preserved. Compared to other reported methods, the MWNTs in our research are better suited to form a conducting interconnected nanotube network in the polymer matrix, to which we attribute the low nanotube loading threshold for the formation of a conductive network.

Moreover, the absolute conductivities of our MWNT/PI composites are much higher than the reported values of CNT/PI composites with the same nanotube loading. For example, for nanotube/polyimide composites with 5 wt % nanotubes, the reported conductivities are in the range of 10^{-9}−10^{-4} S cm^{-1},[10−12,14,38,39] which is ∼3−8 orders of magnitude lower than our value (0.27 S cm^{-1}). Our conductivity reaches 13.3 S cm^{-1} at 20 wt % MWNT loading and 38.8 S cm^{-1} at 30 wt % MWNT loading, which is ∼17 orders of magnitude higher than that of neat PI. These values are the highest values reported yet for CNT/PI composites.[11,12,39] The electrical conductivity of the composite with 30 wt % MWNTs (38.8 S cm^{-1}), to the best of our knowledge, is the highest value ever reported for a solution-processed nanotube composite. The electrical conductivity of our MWNT/PI composites is tunable from 10^{-16} S cm^{-1} to 38.8 S cm^{-1} by varying the nanotube content. At a loading of 0.75 wt %, the conductivity reaches 7.2×10^{-5} S cm^{-1}, which satisfies the requirements of electrostatic dissipation applications (10^{-5} S cm^{-1}). The conductivity of the composite with 5 wt % MWNTs (0.27 S cm^{-1}) is adequate for electromagnetic interference (EMI) shielding applications (0.1 S cm^{-1}).

Mechanical Properties. The tensile properties of neat PI and MWNT/PI composite films with various MWNT loadings are summarized in Table 1 and Figure 10. Figure 10a presents representative stress−strain curves. For neat PI films, the tensile modulus is 6.37 ± 0.13 GPa and the strength is 151.2 ± 5.1 MPa. The reported tensile values of polyimide vary widely, since they are dependent on the diamine and dianhydride used. Our modulus and strength are in the higher end of the published range, because of the rigid monomers that we employed.[11,12,40] As shown in Figures 10b and 10c, an increase in MWNT loading from 0 wt % to 10 wt % leads to a continuous increase of both tensile modulus and strength. Increasing the MWNT loading

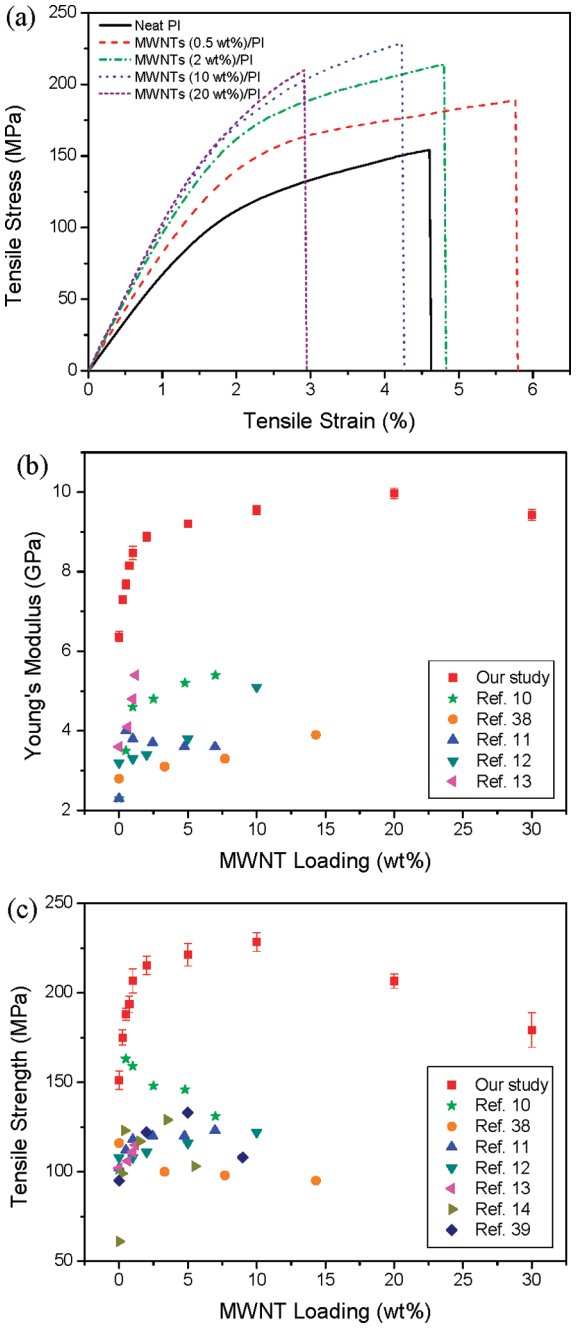

Figure 10. (a) Representative stress−strain curves of neat PI and MWNT/PI composites with MWNT loadings of 0.5, 2, 10, and 20 wt %. Comparison of (b) Young's modulus and (c) tensile strength of composites prepared in this study with published values for other CNT/PI composites. The tensile data for other CNT/PI composites were reprinted with permission from these noted references.

dx.doi.org/10.1021/cm200909x |*Chem. Mater.* 2011, 23, 4149–4157

further to 20 and 30 wt % results in a decrease in tensile modulus and strength. This can be attributed to the reduced distance between nanotubes (Figure 7f), which would cause highly intensified stress field between the closely spaced nanotubes[41] and increased free volume.[42] However, the MWNT(30 wt %)/PI composite still has improved tensile properties (with a modulus of 9.43 ± 0.14 GPa and a strength of 179.2 ± 9.7 MPa), compared to the unreinforced matrix (with respective values of 6.37 ± 0.13 GPa and 151.2 ± 5.1 MPa). Figures 10b and 10c also show comparison of our tensile properties with the values recently reported in the literature for CNT/PI composites.[10−14,38,39] Our absolute tensile values at all nanotube loadings investigated (6−10 GPa and 151−228 MPa) are higher than the reported Young's modulus and tensile strength of other CNT/PI composites, which are in the range of 3−5 GPa and 100−130 MPa, respectively.

We believe that the excellent electrical conductivity and mechanical properties achieved in this study are due to the high CNT dispersion efficacy of the designed PAA, which functions both as the polymer matrix precursor and as the nanotube dispersant. The PAA has good affinity for the nanotubes and also good solubility in the solvent. It interacts noncovalently with nanotube surface without severe damage to their length and conjugated π system. A single polymer functioning as both a matrix precursor and a dispersant avoids any incompatibility issue between the matrix and the dispersant, such as that which has been encountered in some other studies. As a result, high mechanical properties were obtained for the composite with high nanotube loading. The MWNTs can be uniformly dispersed throughout the PI matrix at high nanotube content, leading to more effective electrical network formation and increased electrical conductivity.

MWNT/PI Coatings. Besides highly electrically conductive and mechanically strong free-standing composite films, the PAA-functionalized MWNT dispersions can also be used to fabricate composite coatings on various substrates. Figure 2g shows a transparent coating of MWNT (30 wt %)/PI on a glass substrate prepared via the spraying process. The measured transmittance of this coating is 81% ± 0.4% at 550 nm, which is calculated based on 10 transmission scans of this coating at different spots. The extremely low standard deviation, compared to the mean transmittance value, indicates the very high uniformity of our composite coating. Similar ultrathin composite coating (several hundreds of nm) can also be deposited on an aluminum substrate. Thicker coatings (given in micrometers) on aluminum (see Figure 2h) can be prepared by solution casting, because of their excellent adhesion to aluminum. Unlike neat nanotube coatings, which may be peeled off because of their weak adhesion to the substrates, our composite coatings have good stability and can be easily handled. Combined with their high electrical conductivity (~38.8 S cm^{-1}), as well as high temperature resistance and good chemical-resistant properties, they may have wide applications in electronics and aerospace industries.

CONCLUSIONS

In summary, we have synthesized a rigid hydroxyl-functionalized poly(amic acid) (PAA), which is the precursor of polyimide, and have demonstrated its ability to perform the dual functions of a highly effective dispersant of MWNTs and a matrix material for polymer/MWNT composites. MWNT/PI composite films made by the conventional solution casting technique with this dual-function PAA show outstanding electrical properties. The electrical conductivity of the composites reaches 38.8 S cm^{-1} at a MWNT loading of 30 wt % and the nanotube concentration for the percolation threshold of conductivity of MWNT/PI composites is 0.48 wt %, which are, respectively, the highest and among the lowest reported values for any conventional solution-processed nanotube composites. The 30 wt % MWNT composite has higher Young's modulus (9.43 ± 0.14 GPa) and tensile strength (179.2 ± 9.7 MPa) values than common polyimides. To the best of our knowledge, this is also the first report of MWNT/PI composites with MWNT loadings as high as 30 wt % made by the solution casting technique, which is a simple and commonly employed method. The excellent electrical and mechanical properties, combined with the facile fabrication technique, make this MWNT/PI composite a promising material for many potential applications, such as electrostatic dissipation, electromagnetic interference shielding, and flexible printed circuit boards. Uniform and stable MWNT(30 wt %)/PI composite coatings have also been deposited on glass and aluminum substrates.

ASSOCIATED CONTENT

Supporting Information. Optical micrograph of MWNT (30 wt %)/PAA film; FT-IR spectra of MWNTs, PAA, and MWNT/PAA complex; TGA curves of MWNTs, PAA, and MWNT/PAA complex; DSC curve of PAA film; and optical micrographs of MWNT/PI composite films. This materials is available free of charge via the Internet at http://pubs.acs.org.

AUTHOR INFORMATION

Corresponding Author
*Phone: +65 63168938. E-mail: mbechan@ntu.edu.sg.

ACKNOWLEDGMENT

The authors gratefully acknowledge financial support of the Defense & Science Technology Agency of Singapore (No. POD0513240) and Singapore National Research Foundation through a Competitive Research Program grant (No. NRF-CRP2-2007-02). We thank Dr. G. Poernomo for his help in TEM measurements. W. Yuan thanks Nanyang Technological University for the support of her Ph.D. scholarship.

REFERENCES

(1) Moniruzzaman, M.; Winey, K. I. *Macromolecules* **2006**, *39*, 5194–5205.
(2) Spitalsky, Z.; Tasis, D.; Papagelis, K.; Galiotis, C. *Prog. Polym. Sci.* **2010**, *35*, 357–401.
(3) Ramasubramaniam, R.; Chen, J.; Liu, H. Y. *Appl. Phys. Lett.* **2003**, *83*, 2928–2930.
(4) Bryning, M. B.; Islam, M. F.; Kikkawa, J. M.; Yodh, A. G. *Adv. Mater.* **2005**, *17*, 1186–1191.
(5) Blighe, F. M.; Hernandez, Y. R.; Blau, W. J.; Coleman, J. N. *Adv. Mater.* **2007**, *19*, 4443–4447.
(6) Luo, C.; Zuo, X. L.; Wang, L.; Wang, E. G.; Song, S. P.; Wang, J.; Fan, C. H.; Cao, Y. *Nano Lett.* **2008**, *8*, 4454–4458.
(7) Munoz, E.; Suh, D. S.; Collins, S.; Selvidge, M.; Dalton, A. B.; Kim, B. G.; Razal, J. M.; Ussery, G.; Rinzler, A. G.; Martinez, M. T.; Baughman, R. H. *Adv. Mater.* **2005**, *17*, 1064–1067.
(8) Grossiord, N.; Loos, J.; van Laake, L.; Maugey, M.; Zakri, C.; Koning, C. E.; Hart, A. J. *Adv. Funct. Mater.* **2008**, *18*, 3226–3234.

(9) Jiang, X. W.; Bin, Y. Z.; Matsuo, M. *Polymer* **2005**, *46*, 7418–7424.
(10) Yuen, S. M.; Ma, C. C. M.; Chiang, C. L.; Teng, C. C.; Yu, Y. H. *J. Polym. Sci., Part A: Polym. Chem.* **2008**, *46*, 803–816.
(11) Yuen, S. M.; Ma, C. C. M.; Chiang, C. L.; Lin, Y. Y.; Teng, C. C. *J. Polym. Sci., Part A: Polym. Chem.* **2007**, *45*, 3349–3358.
(12) Isayev, A. I.; Kumar, R.; Lewis, T. M. *Polymer* **2009**, *50*, 250–260.
(13) Wu, D. C.; Shen, L.; Low, J. E.; Wong, S. Y.; Li, X.; Tjiu, W. C.; Liu, Y.; Bin He, C. *Polymer* **2010**, *51*, 2155–2160.
(14) Lebron-Colon, M.; Meador, M. A.; Gaier, J. R.; Sola, F.; Scheiman, D. A.; McCorkle, L. S. *ACS Appl. Mater. Interfaces* **2010**, *2*, 669–676.
(15) Yuan, W.; Feng, J.; Judeh, Z.; Dai, J.; Chan-Park, M. B. *Chem. Mater.* **2010**, *22*, 6542–6554.
(16) Yan, Y. H.; Chan-Park, M. B.; Zhou, Q.; Li, C. M.; Yue, C. Y. *Appl. Phys. Lett.* **2005**, *87*, 213101.
(17) Chen, J.; Liu, H. Y.; Weimer, W. A.; Halls, M. D.; Waldeck, D. H.; Walker, G. C. *J. Am. Chem. Soc.* **2002**, *124*, 9034–9035.
(18) Ikeda, A.; Nobusawa, K.; Hamano, T.; Kikuchi, J. *Org. Lett.* **2006**, *8*, 5489–5492.
(19) Chen, J.; Ramasubramaniam, R.; Xue, C.; Liu, H. *Adv. Funct. Mater.* **2006**, *16*, 114–119.
(20) Zou, J. H.; Liu, L. W.; Chen, H.; Khondaker, S. I.; McCullough, R. D.; Huo, Q.; Zhai, L. *Adv. Mater.* **2008**, *20*, 2055–2060.
(21) Tchoul, M. N.; Ford, W. T.; Ha, M. L. P.; Chavez-Sumarriva, I.; Grady, B. P.; Lolli, G. L.; Resasco, D. E.; Arepalli, S. *Chem. Mater.* **2008**, *20*, 3120–3126.
(22) Baskaran, D.; Mays, J. W.; Bratcher, M. S. *Chem. Mater.* **2005**, *17*, 3389–3397.
(23) Gu, H.; Swager, T. M. *Adv. Mater.* **2008**, *20*, 4433–4437.
(24) Delozier, D. M.; Watson, K. A.; Smith, J. G.; Clancy, T. C.; Connell, J. W. *Macromolecules* **2006**, *39*, 1731–1739.
(25) Saini, V.; Li, Z.; Bourdo, S.; Dervishi, E.; Xu, Y.; Ma, X.; Kunets, V. P.; Salamo, G. J.; Viswanathan, T.; Biris, A. R.; Saini, D.; Biris, A. S. *J. Phys. Chem. C* **2009**, *113*, 8023–8029.
(26) Chen, B. K.; Tsai, Y. J.; Tsay, S. Y. *Polym. Int.* **2006**, *55*, 93–100.
(27) Tullos, G. L.; Mathias, L. J. *Polymer* **1999**, *40*, 3463–3468.
(28) Hasan, T.; Scardaci, V.; Tan, P. H.; Rozhin, A. G.; Milne, W. I.; Ferrari, A. C. *J. Phys. Chem. C* **2007**, *111*, 12594–12602.
(29) Clark, M. D.; Krishnamoorti, R. *J. Phys. Chem. C* **2009**, *113*, 20861–20868.
(30) Yuan, J. M.; Fan, Z. F.; Chen, X. H.; Wu, Z. J.; He, L. P. *Polymer* **2009**, *50*, 3285–3291.
(31) Liu, T. X.; Phang, I. Y.; Shen, L.; Chow, S. Y.; Zhang, W. D. *Macromolecules* **2004**, *37*, 7214–7222.
(32) Kim, K. H.; Jo, W. H. *Macromolecules* **2007**, *40*, 3708–3713.
(33) Rao, A. M.; Eklund, P. C.; Bandow, S.; Thess, A.; Smalley, R. E. *Nature* **1997**, *388*, 257.
(34) Zhou, B.; Lin, Y.; Hill, D. E.; Wang, W.; Veca, L. M.; Qu, L. W.; Pathak, P.; Meziani, M. J.; Diaz, J.; Connell, J. W.; Watson, K. A.; Allard, L. F.; Sun, Y. P. *Polymer* **2006**, *47*, 5323–5329.
(35) Lin, Y.; Taylor, S.; Huang, W. J.; Sun, Y. P. *J. Phys. Chem. B* **2003**, *107*, 914–919.
(36) Sun, Y. P.; Fu, K. F.; Lin, Y.; Huang, W. J. *Acc. Chem. Res.* **2002**, *35*, 1096–1104.
(37) Garboczi, E. J.; Snyder, K. A.; Dongks, J. E.; Thorpe, M. F. *Phys. Rev. E* **1995**, *52*, 819.
(38) Ogasawara, T.; Ishida, Y.; Ishikawa, T.; Yokota, R. *Composites, Part A* **2004**, *35*, 67–74.
(39) Zhu, B. K.; Xie, S. H.; Xu, Z. K.; Xu, Y. Y. *Compos. Sci. Technol.* **2006**, *66*, 548–554.
(40) Smith, J. G.; Connell, J. W.; Delozier, D. M.; Lillehei, P. T.; Watson, K. A.; Lin, Y.; Zhou, B.; Sun, Y. P. *Polymer* **2004**, *45*, 825–836.
(41) Broek, D. *Elementary Engineering Fracture Mechanics*; Kluwer Academic Publishers: Dordrecht, The Netherlands, 1986.
(42) An, L.; Pan, Y. Z.; Shen, X. W.; Lu, H. B.; Yang, Y. L. *J. Mater. Chem.* **2008**, *18*, 4928–4941.